MOLECULAR IMAGING AND BIOLOGY

Mol Imaging Biol (2017) 19:90–99
DOI: 10.1007/s11307-016-0987-0

Published Online: 18 July 2016

RESEARCH ARTICLE

CD80 Is Upregulated in a Mouse Model with Shear Stress-Induced Atherosclerosis and Allows for Evaluating CD80-Targeting PET Tracers

Romana Meletta,[1] Larissa Steier,[1] Nicole Borel,[2] Linjing Mu,[3] Claudia Keller,[1] Aristeidis Chiotellis,[1] Erica Russo,[1] Cornelia Halin,[1] Simon M. Ametamey,[1] Roger Schibli,[1,3] Stefanie D. Krämer,[1] Adrienne Müller Herde[1]

[1]*Department of Chemistry and Applied Biosciences, ETH Zurich, Vladimir-Prelog-Weg 1-5/10, 8093, Zurich, Switzerland*
[2]*Institute of Veterinary Pathology, Vetsuisse Faculty, University of Zurich, Winterthurerstrasse 268, 8057, Zurich, Switzerland*
[3]*Department of Nuclear Medicine, University Hospital Zurich, 8091, Zurich, Switzerland*

Abstract

Purpose: A shear stress-induced atherosclerosis mouse model was characterized for its expression of inflammation markers with focus on CD80. With this model, we evaluated two positron emission tomography (PET) radiotracers targeting CD80 as well as 2-deoxy-2-[^{18}F]fluoro-D-mannose ([^{18}F]FDM) in comparison with 2-deoxy-2-[^{18}F]fluoro-D-glucose ([^{18}F]FDG).

Procedure: A flow constrictive cuff implanted around the common carotid artery in apolipoprotein E knockout mice resulted in plaque formation. CD80 expression levels and plaque histopathology were evaluated. Serial PET/X-ray computed tomography scans were performed to follow inflammation.

Results: Plaque formation with increased levels of CD80 was observed. Histologically, plaques presented macrophage-rich and large necrotic areas covered by a thin fibrous cap. Of the CD80-specific tracers, one displayed an increased uptake in plaques by PET. Both [^{18}F]FDG and [^{18}F]FDM accumulated in atherosclerotic plaques.

Conclusion: This mouse model presented, similar to humans, an increased expression of CD80 which renders it suitable for non-invasively targeting CD80-positive immune cells and evaluating CD80-specific radiotracers.

Key words: Positron emission tomography, Atherosclerosis, CD80, ApoE KO, Shear stress, Plaque inflammation, [^{18}F]FDG

Abbreviations: [^{18}F]FDG, 2-deoxy-2-[^{18}F]fluoro-D-glucose; [^{18}F]FDM, 2-deoxy-2-[^{18}F]fluoro-D-mannose; ApoE, Apolipoprotein E; DS, Downstream; FACS, Fluorescence-activated cell sorting; HFD, High-fat diet; KO, Knockout; ND, Normal diet; PET, Positron emission tomography; SUV, Standardized uptake value; US, Upstream

Introduction

Atherosclerosis is an inflammatory disease affecting preferentially arterial segments exposed to oscillatory or low-shear stress conditions as they often occur near bifurcations or in inner curvatures of arteries [1–4].

Electronic supplementary material The online version of this article (doi:10.1007/s11307-016-0987-0) contains supplementary material, which is available to authorized users.

Correspondence to: Adrienne Müller Herde; *e-mail:* adrienne.herde@pharma.ethz.ch

Atherosclerotic lesions evolve over decades and can eventually form vulnerable plaques that are prone to rupture. Subsequent thrombus formation results in reversible ischemic episodes or even complete occlusions of arteries, thereby impairing the function of downstream tissues and organs. This can cumulate in life-threatening conditions such as a myocardial infarction or stroke.

Positron emission tomography (PET) is a non-invasive imaging technique providing quantitative information about functional processes. Together with computed tomography (CT) or magnetic resonance imaging supplying anatomical information, PET allows investigating three-dimensional, dynamic distribution patterns of radiotracers *in vivo* at excellent sensitivity. Therefore, PET has high potential to become a meaningful tool for the risk assessment of atherosclerotic plaques. The metabolic PET tracer 2-deoxy-2-[^{18}F]fluoro-D-glucose ([^{18}F]FDG) is a clinically established radiotracer in oncology and moreover accumulates at sites of active inflammation including atherosclerotic plaques. In atherosclerosis, studies demonstrated that the uptake of [^{18}F]FDG in plaques of patients correlated with the inflammatory and disease activity [5, 6]. However, [^{18}F]FDG non-specifically accumulates at systemic sites of inflammation and in regions of high metabolic activity such as the myocardium. Therefore, a more selective radiotracer specifically binding to both coronary and carotid plaques would present a significant progress towards clinical atherosclerosis imaging. Research efforts have focused on the identification of targets involved among others in plaque inflammation [7, 8], angiogenesis [9], and calcifications [10].

Our own efforts are directed towards the development of radiotracers targeting the T lymphocyte activation antigen CD80. The expression of CD80 by activated antigen-presenting cells is increased in vulnerable compared to stable human carotid plaques [11]. We have previously published the development and *in vitro* and *in vivo* characterization of the pyrazolocinnoline derivative [^{11}C]AM7 (Fig. 1a) [11]. This CD80-targeting radiotracer candidate shows nanomolar affinity to human CD80 and bound *in vitro* to human atherosclerotic plaques but was not yet evaluated in an animal model of atherosclerosis.

Rodent atherosclerosis models for preclinical radiotracer evaluation are primarily based on genetically modified animals in combination with a diet enriched with cholesterol and fat to make the animals susceptible to atherosclerosis. A recently described approach by Cheng et al. is based on this principle but additionally takes into account the impact of blood flow dynamics on plaque development [12]. In this shear stress-controlled murine atherosclerosis model, a flow constrictive device, referred to as a cuff, is placed around the common carotid artery of apolipoprotein E knockout (ApoE KO) mice fed with a high-fat diet (HFD). The implanted cuff leads to defined altered flow conditions giving rise to the formation of atherosclerotic lesions upstream (US) and downstream (DS) of the cuff [12–15]. In fact, two previous studies investigated the accumulation of radiotracers, including [^{18}F] FDG), in plaques of this mouse model [15, 16].

In this model, we implanted into ApoE KO mice fed a HFD a flow-constrictive cuff around the right common carotid artery (cuff carotid) and a non-constrictive control around the carotid on the contralateral side (control carotid). Both implants show good contrast in CT and make the localization of the cuff and control carotids convenient in PET/CT images. The goal of this study was to characterize this mouse model, which we refer to as ApoE KO-cuff mouse model, regarding the gene and protein expression of relevant inflammatory mediators, in particular CD80, in comparison with its blood lipid profile, plaque development, and morphology. As the inflammation marker CD80 and the macrophage mannose receptor (MMR) were upregulated in atherosclerotic lesions, we further investigated the accumulation of the CD80-targeting [^{11}C]AM7 and the MMR-targeting 2-

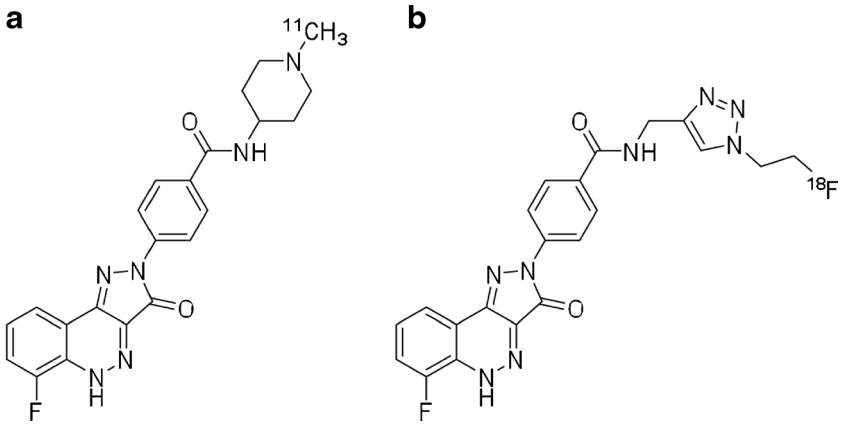

Fig. 1. Structures of CD80 PET radiotracers: **a** [^{11}C]AM7 and **b** [^{18}F]AC74.

deoxy-2-[^{18}F]fluoro-D-mannose ([^{18}F]FDM) [17] in comparison with the gold standard for inflammation imaging, [^{18}F]FDG.

Materials and Methods

For materials and methods, see supplementary information.

Results

Body Weight and Blood Lipid Profile

Mouse body weight and blood lipids were analyzed in wild-type C57BL/6-cuff mice on normal diet (C57BL/6-cuff ND), ApoE KO-cuff ND, and ApoE KO-cuff HFD mice over 5 months (Fig. 2, Table S1). At study beginning, wild-type mice showed a significantly higher body weight than ApoE KO mice; however, a similar increase in weight over time was observed for all groups. Compared to wild-type mice, ApoE KO-cuff ND animals showed significantly increased total cholesterol, high-density lipoprotein (HDL), and low-density lipoprotein (LDL) values whereas no significant increase was observed for the triglycerides. The ApoE KO-cuff HFD mice displayed a significant increase in all analyzed blood lipids compared to C57BL/6-cuff ND mice. In ApoE KO-cuff mice, the levels of total cholesterol, triglycerides, and LDL were significantly higher in animals fed a HFD than ND. Blood lipids increased in ApoE KO-cuff HFD animals right after the onset of the HFD.

Visualization of Intravascular Lipid Deposits

The development of atherosclerotic plaques was evaluated by lipid staining of dissected aortas and carotids of ApoE KO-cuff HFD mice at defined time points after surgery (6, 8, 13, and 17 weeks). Over time, an increasing plaque burden was observed with initial lesions found in the aortic arch, followed by plaques in the bifurcations of the carotids and close to both implants (Fig. 3). In the cuff segment, plaques were observed DS and US; however, in some exceptional cases, no plaques developed US of the cuff. In the control carotid, the lipid staining was unexpectedly positive DS and, in approximately 32 % of the animals, also US of the control implant (data not shown). In addition, ApoE KO-cuff ND mice showed atherosclerotic plaque development predominantly in the aortic arch whereas control C57BL/6-cuff ND mice were not affected by atherosclerosis 18 weeks post surgery (Fig. S3).

Histological Evaluation of the Carotid, Aortic, and Coronary Arteries of ApoE KO-Cuff Mice

The development of atherosclerotic plaques in the vasculature of ApoE KO-cuff mice was investigated by hematoxylin/eosin (HE) staining and CD68 immunohistochemistry at defined

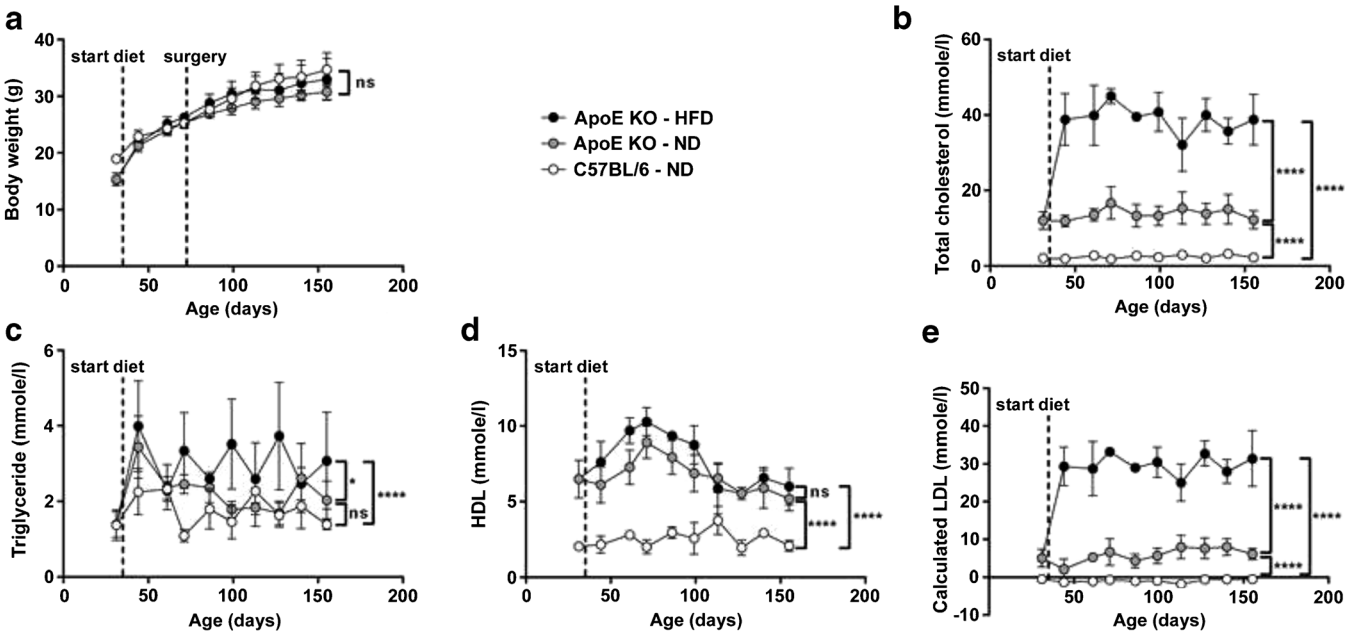

Fig. 2. **a** Body weight, **b** total cholesterol, **c** triglycerides, **d** HDL, and **e** LDL in ApoE KO-cuff mice fed a HFD or ND and in C57BL/6-cuff mice on ND. The values indicate mean ± SD of $n = 3$ animals per time point per group (not identical animals at each time point). *Dashed lines* mark the HFD onset (ApoE KO HFD) and the surgery (all groups), respectively. *ns* non-significant; $^{*}p < 0.05$; $^{****}p < 0.0001$. The values are additionally listed in Table S1.

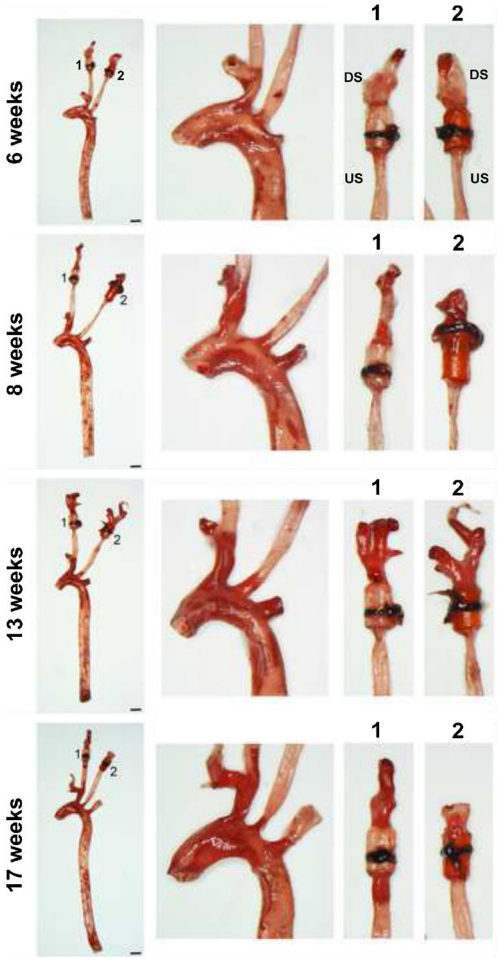

Fig. 3. Representative oil red o staining (lipids) of the aorta and carotids of ApoE KO-cuff HFD mice 6, 8, 13, and 17 weeks after surgery. The magnified images show the aortic arch, the cuff carotid, and the control carotid. *1* cuff; *2* control; *DS* downstream, *US* upstream. *Scale bars* = 1 mm.

time points post surgery (6, 9, 16, and 18 weeks) (Fig. 4, Figs. S4–S7). Analysis of structural and compositional features of plaques US and DS of the cuff and control implants over time revealed large, complex, and heterogeneous lesions containing CD68-positive cells (Fig. 4, Fig. S5). At early time points, occasionally fatty streaks were noted. No plaques were observed within the cuff; however, small atherosclerotic lesions were detected within the control implant at late time points.

The lesion size, defined as the intima-to-media ratio, at 18 weeks post surgery reached 2.9 ± 0.4 DS and 3.9 ± 0.9 US of the cuff. The ratios were 3.2 ± 0.6 DS and 1.7 ± 0.4 US for the control. Besides an expanded plaque size, enlarged necrotic core (NC) and thin fibrous cap (FC) define plaque vulnerability. NC formation (% of intima) was more pronounced in the cuff than control region. DS and US of the cuff, the NC covered 11.3 ± 1.8 and 15.3 ± 2.3 %, respectively, and DS and US of the control, it covered 2.9 ± 0.5 and 7.3 ± 0.8 %, respectively. The earliest time point a FC could be determined was at 16 weeks and did not change significantly until 18 weeks in both cuff and control. The averaged FC thicknesses were 33 ± 6 and 17 ± 4 μm DS and US of the cuff and 36 ± 6 and 38 ± 7 μm DS and US of the control, respectively. As compositional feature, CD68-positive areas were quantified which increased steadily over time reaching 15.4 ± 1.7 and 17.6 ± 1.2 % DS and US of the cuff and 9.4 ± 0.9 and 11.0 ± 1.0 % DS and US of the control, respectively. In none of the lesions, intraplaque hemorrhage (IPH) was detected. Histopathologically, advanced plaques presented a heterogeneous structure, large necrotic portions, an overall high inflammatory activity, and a thin and unstructured fibrous cap without IPH. Overall, no distinct difference in morphology was noted between plaques located US and DS of the cuff. A perivascular inflammation, probably due to the implants, was present in all examined sections with numerous CD68-positive inflammatory cells around the vessel.

In the aorta of ApoE KO-cuff mice, plaque burden and complexity increased over time (Fig. S6). At 18 weeks post surgery, plaques covered large parts of the aorta, thereby narrowing the vessel lumen. Lesion appears with focal accumulations of cholesterol crystals, immune cells including foam cells, and lipid droplets. Arterial vessels originating from the heart and aortic valves of ApoE KO-cuff mice were heavily affected by atherosclerotic lesions, but coronary arteries were not (Fig. S7).

CD68, CD80, and MRC1 Gene Expression and CD80 Protein Expression in ApoE KO and Control Mice

The gene expression of inflammatory mediators was investigated in the aortic arch, descending aorta, cuff segments, control segments, heart, spleen, and thymus of ApoE KO-cuff HFD, ApoE KO-cuff ND, and C57BL/6-cuff ND mice by quantitative PCR (qPCR) at 18 weeks after cuff or control implantation (Fig. 5a–c, Figs. S8–S10). The aortic arch displayed significantly increased messenger RNA (mRNA) levels of CD68, CD80, and the macrophage mannose receptor (*MRC1 gene*), which are all expressed by macrophages, compared to wild-type mice (Fig. 5a–c). Moreover, a significantly higher CD68 expression in ApoE KO-cuff than wild-type mice was present in other segments affected by atherosclerosis, *e.g.*, the descending aorta and the vascular segments US and DS of the cuff and control (Fig. S8). The difference in CD80 expression was significant in the aorta, the cuff segments, and the heart (Fig. S9). There was no upregulation of MRC1 expression in these regions (Fig. S10). Comparing expression levels over time in ApoE KO-cuff HFD mice 9, 12, 15, 17, and 18 weeks post surgery (Figs. S11–S13), only CD68 expression was increased.

To analyze CD80 protein expression, fluorescence-activated cell sorting (FACS) was performed on single cell suspensions generated from the combined aorta and carotids of ApoE KO HFD or ApoE KO ND animals (Fig. 5d, e). In

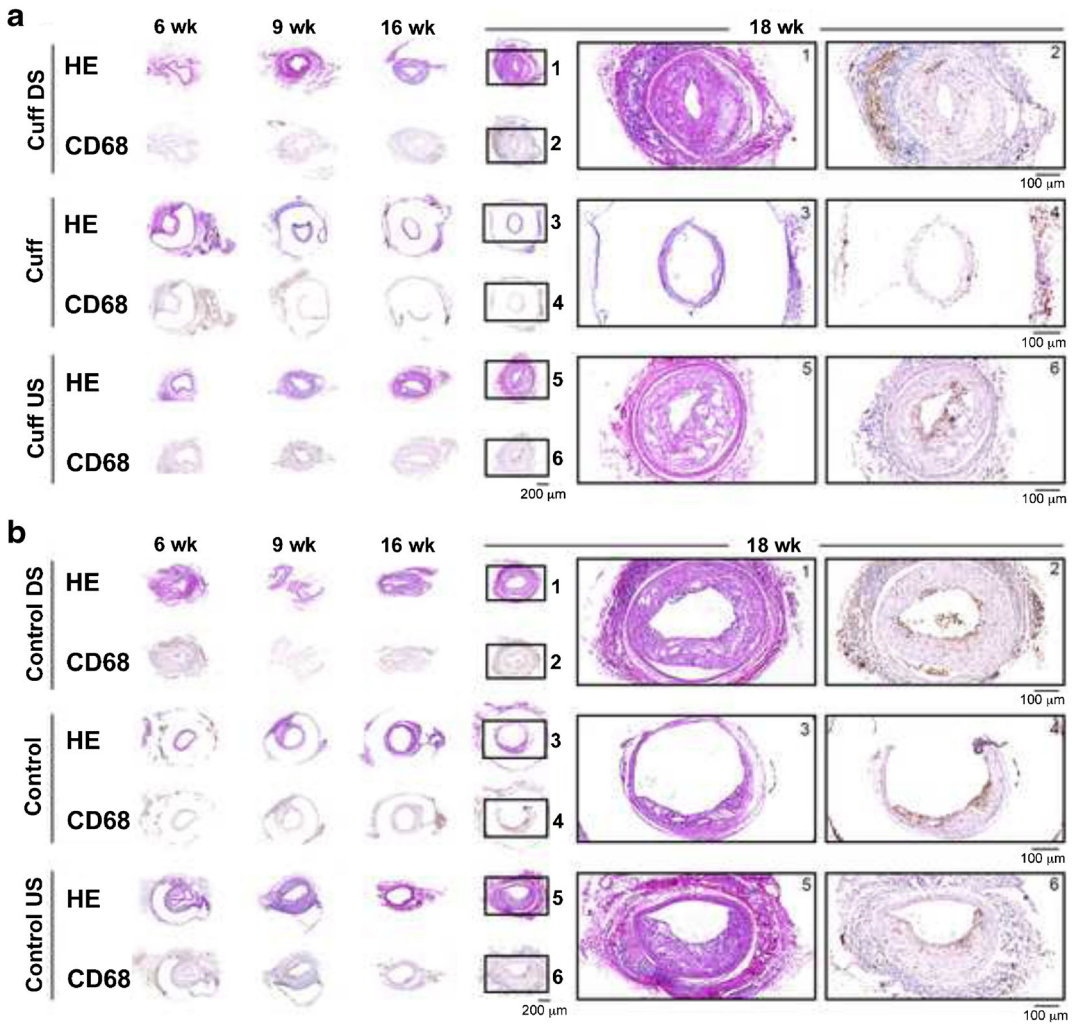

Fig. 4. Representative hematoxylin/eosin (*HE*) and CD68 immunohistochemistry images of the segments DS, within, and US of the cuff (**a**) and the control (**b**) in ApoE KO-cuff HFD mice 6, 9, 16, and 18 weeks (*wk*) post surgery. Higher magnification images show vascular regions with lipid- and cholesterol crystal-rich plaques, necrotic areas, and thin fibrous caps; *1* and *2* indicate DS, *3* and *4* within, and *5* and *6* US.

line with our gene expression measurements, ApoE KO HFD mice presented significantly higher CD80 protein levels than animals on ND as judged from the delta median fluorescence intensity plot (Fig. 5e).

In Vivo Radiotracer Evaluation in the Cuff Carotid of ApoE KO-Cuff HFD Mice by PET/CT

In vivo PET/CT scans of ApoE KO-cuff mice were acquired 9, 12, and 15 weeks after surgery. The time points for imaging were chosen based on the time course of plaque development and the time needed to reduce post-surgical inflammation in this mouse model as assessed by [^{18}F]FDG (data not shown). ApoE KO-cuff HFD mice were injected with either [^{11}C]AM7 or [^{18}F]AC74 (Fig. 1b), a fluorine-18 labeled analog of [^{11}C]AM7 with 10-fold lower binding affinity to hCD80 (A. Chiotellis *et al.*, manuscript in prep.), or [^{18}F]FDM, and every mouse was additionally scanned with [^{18}F]FDG. This resulted in a higher number of animals scanned with [^{18}F]FDG than with the other tracers. For the CD80-specific tracer [^{11}C]AM7, a higher standardized uptake value (SUV) in both US and DS plaques of the cuff than the background (neck) region was observed at all three time points, indicating an accumulation in atherosclerotic plaques (Figs. 6 and 7). Differences were significant at 9 weeks after surgery. The uptake of the CD80 radiotracer candidate [^{18}F]AC74 was similar in plaque and background regions and was independent of the time point. Even at later time points (19 weeks after surgery), when plaque size increased more, [^{18}F]AC74 did not significantly accumulate in plaques (data now shown). [^{18}F]FDG and [^{18}F]FDM displayed significantly higher SUV values in the cuff US and DS segments than the background. A significant difference in SUV values between the US and DS segments was only determined for [^{18}F]FDG 12 weeks after surgery,

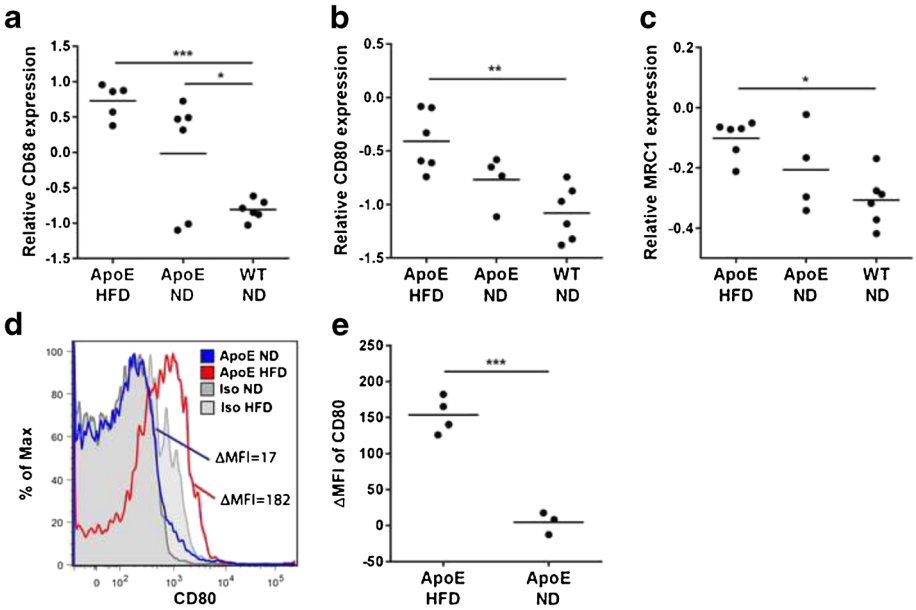

Fig. 5. Relative gene expression in the aortic arch of ApoE KO-cuff HFD, ApoE KO-cuff ND, and C57BL/6 (WT)-cuff ND mice at 18 weeks post surgery for CD68 (**a**), CD80 (**b**), and MRC1 (**c**). **d** FACS analysis of CD80 expression among all $CD45^+$ cells present in single cell suspensions generated from the aorta and carotids. A representative histogram plot is shown, which reveals an increased CD80 delta median fluorescence intensity (*ΔMFI*) in ApoE HFD mice as compared to ApoE KO ND mice. *Iso* isotype control antibody; $\Delta MFI = MFI_{(sample)} - MFI_{(isotype)}$. **e** Quantification of CD80 ΔMFIs measured in all samples. Each *dot* represents one mouse ($n = 3–4$). *Lines* indicate the mean values per group. $^*p < 0.05$; $^{**}p < 0.01$; $^{***}p < 0.001$.

with higher uptake in the US segment. The quantification of tracer accumulation in the aortic arch was hampered by the radioactivity spill over from the high liver uptake of [^{11}C]AM7 and [^{18}F]AC74 and high myocardial uptake of [^{18}F]FDG and [^{18}F]FDM, respectively.

Ex vivo PET imaging was carried out with ApoE KO-cuff HFD mice 18 weeks after surgery to verify [^{18}F]FDG and [^{18}F]FDM uptake in atherosclerotic plaques. After tracer injection, animals were perfused and the dissected vessels were scanned by PET. Both radiotracers accumulated predominantly in the aortic arch, in parts of the descending aorta, and in the carotid segments close to the implanted cuff and control (Fig. S14). Radiotracer binding co-localized with the lipid staining, and plaque-free segments displayed low signals.

Discussion

Preclinical radiotracer evaluation relies on *in vivo* studies in animal models of disease. Currently, there is no consensus about the most appropriate rodent model of atherosclerosis; however, several models have been presented and validated [18–20]. In this study, we demonstrate that the atherosclerotic lesions of the ApoE KO-cuff mouse model initially presented by Cheng et al. [12] contain elevated levels of the inflammation-related markers CD68, CD80, and MMR. Markers that have been identified in human vulnerable plaques were suggested by us and others for atherosclerosis imaging [11, 17]. Subsequently, we evaluated potential radiotracers for the imaging of inflammatory hotspots in this mouse model.

Characterization of the ApoE KO-Cuff Mouse Model

Hyperlipidemia was induced in ApoE KO-cuff mice by feeding a modified Western-type diet, and the entire lipid profile was longitudinally investigated. Lipid levels increased instantly after the HFD onset and remained stable over time. Total cholesterol levels in ApoE KO-cuff mice under HFD or ND were similar to values reported previously [12]. Extensive vascular remodeling processes and plaque development in parallel with changes in inflammatory mediators were observed in this mouse model. Plaque burden in ApoE KO-cuff HFD mice increased over time affecting predominantly the aortic inner curvature and branch points, the US/DS segments of the cuff/control, as well as branch points further DS the carotid arteries, but not the coronary arteries. The implanted constrictive cuff as well as the non-constrictive control led to a significant plaque formation in the adjacent vessel regions, rendering the control implant an inadequate internal control. Plaque development in the control segment was potentially triggered by a perivascular inflammation with cytokine release, vascular damage, or an altered laminar blood flow as described in ApoE*3Leiden mice [21]. In fact, at late time points, plaques appeared within the vessel region covered by

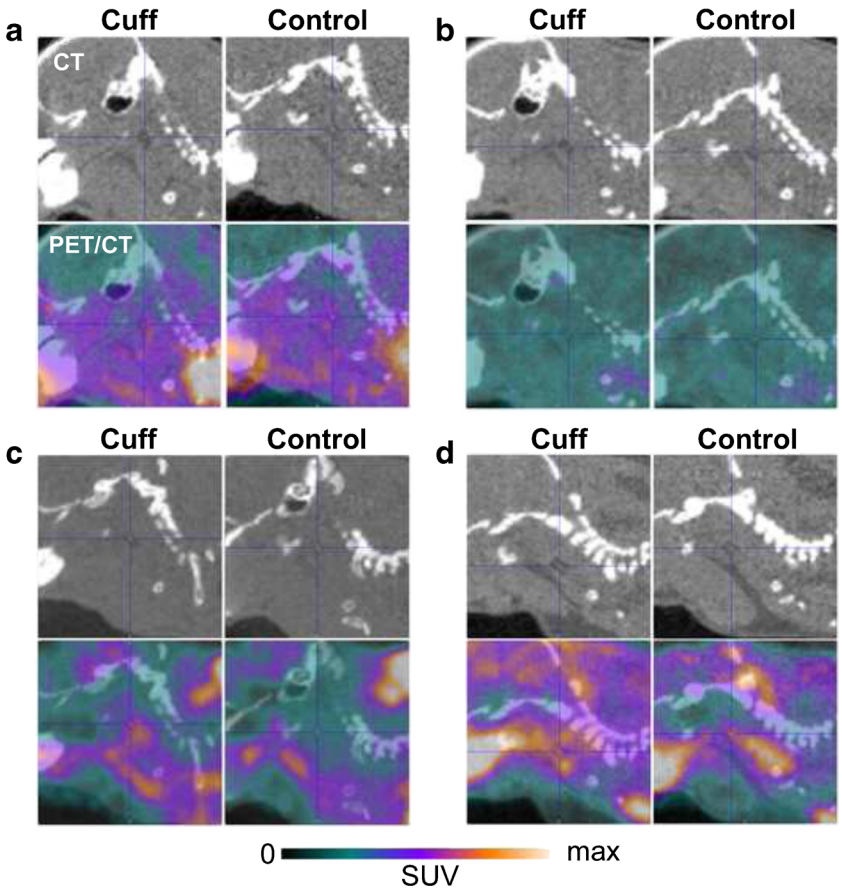

Fig. 6. *In vivo* CT (*gray scale*) and PET/CT slices of the neck region of ApoE KO mice (15 weeks post surgery) after injection of either **a** [^{11}C]AM7, **b** [^{18}F]AC74, **c** [^{18}F]FDG, or **d** [^{18}F]FDM. *Crosshair* indicates cuff and control as clearly visible in CT images. The maximal standardized uptake value (*SUV*) is 0.3 for [^{11}C]AM7 and [^{18}F]AC74 and 0.5 for [^{18}F]FDG and [^{18}F]FDM. Images were averaged from 1 to 61 min post injection of [^{11}C]AM7 and [^{18}F]AC74 and from 30 to 60 min post injection of [^{18}F]FDG and [^{18}F]FDM.

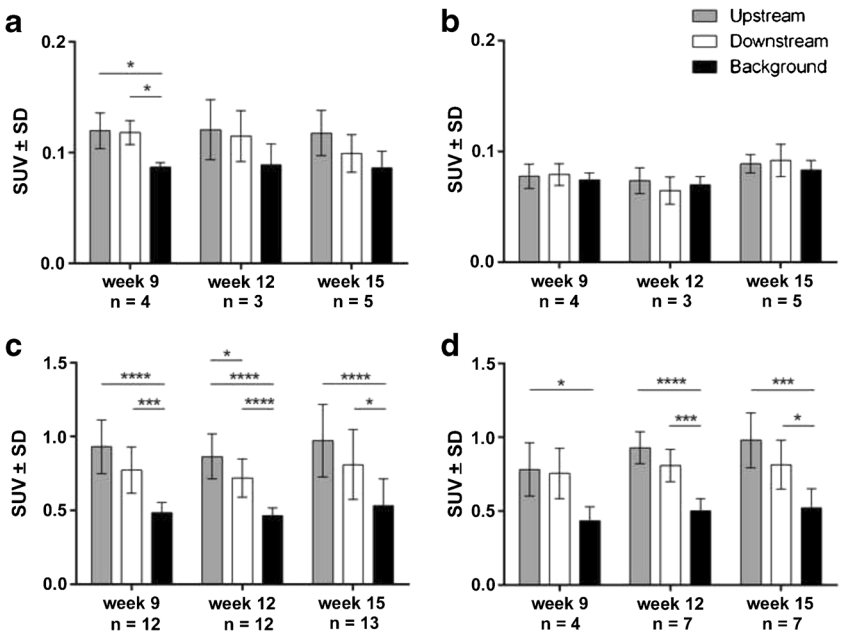

Fig. 7. Radiotracer accumulation (standardized uptake value (*SUV*) ± SD) in the upstream and downstream plaques of the cuff and in the background (muscle neck) in ApoE KO-cuff HFD mice at defined time points after surgery. Evaluated were the CD80-binding tracers **a** [^{11}C]AM7 and **b** [^{18}F]AC74 as well as the metabolic tracers **c** [^{18}F]FDG and **d** [^{18}F]FDM. *n* number of animals scanned. *$p < 0.05$; ***$p < 0.001$; ****$p < 0.0001$.

the non-constrictive control possibly due to the growth of US plaques towards DS, since plaques tend to expand to the direction of lower shear stress [22]. In a future study, a different negative control has to be considered.

By measuring CD80 protein levels in the aorta and carotids by FACS, ApoE KO HFD mice displayed a significantly higher average expression than mice on ND. Since the feeding of a HFD to ApoE KO mice accelerates atherosclerosis development, we postulate that, in this mouse model, CD80 expression correlates with plaque burden and vulnerability as observed *in vitro* in humans [11].

Based on human autopsy studies, vulnerable atherosclerotic plaques are characterized as lesions with thin fibrous caps, large and soft lipid-rich cores, numerous inflammatory cells, and intraplaque hemorrhage [23]. Previous publications described that the plaques generated in this mouse model could be differentiated based on histology and gene expression profiling into stable and vulnerable plaques [12–15, 24]. However, whether or not stable and vulnerable plaques form in this mouse model is still a matter of debate [20, 25, 26]. In our hands, atherosclerotic plaques in this mouse model were classified as advanced lesions independent of the location relative to the implant or of the flow hemodynamics controlled by the different implants. These lesions featured cholesterol crystals, immune cell infiltration with CD68-positive macrophages, focal foam cell accumulations, a large necrotic core, a thin fibrous cap, and constrictive vascular remodeling of heterogeneous organization, however, without intraplaque hemorrhage. A further important feature of human atherosclerosis, the rupture of vulnerable plaques and thereby the occlusion of arterial segments, was not observed in this study in accordance with previous reports [12, 13, 20]. Based on the macrophage number as well as structural and compositional plaque features, no distinct difference of the US compared to the DS cuff segments was observed. Our findings stand in contrast to some previous reports about different plaque phenotypes in this mouse model. Differences in experimental setup, the age of the animals at study beginning, analysis time points, the specific formulation of the diet, the location of the cuff, and a generally high variance in this mouse model could explain the discrepancy.

Independent of a distinction between vulnerable and stable plaques, this mouse model is of interest to investigate advanced and highly inflamed plaques *in vivo* and evaluate molecular imaging strategies. In particular, our target of interest, CD80, was upregulated in the atherosclerotic lesions of this model, allowing the *in vivo* evaluation of CD80-targeting radiotracers.

Radiotracer Evaluation

In this study, the CD80 tracers [^{11}C]AM7 and [^{18}F]AC74 developed in our group were compared to the well-characterized imaging agent [^{18}F]FDG and its stereoisomeric counterpart [^{18}F]FDM. The latter two are metabolic tracers that are transported into the cell by glucose transport proteins (GLUT) and are subsequently phosphorylated and intracellularly trapped [27, 28]. [^{18}F] FDM additionally binds to the MMR (CD206) on the surface of alternatively activated macrophages (M2a) [29]. So far, controversial statements were published regarding the association of MMR-expressing macrophages and plaque phenotype whereas CD80-expressing pro-inflammatory M1 macrophages are unambiguously linked to plaque vulnerability [17, 30–32].

Ex vivo [^{18}F]FDG and [^{18}F]FDM accumulation was found in areas of atherosclerotic plaques in the aorta and carotids of ApoE KO-cuff HFD mice. *In vivo*, we observed higher [^{18}F]FDG and [^{18}F]FDM accumulation US than DS which is, for [^{18}F]FDG, in line with the study by Wenning et al. [15]. They observed significant differences at all examined time points in contrast to our results. Based on our histological analysis revealing a similar plaque phenotype US and DS of the cuff, the minor difference in accumulation between these segments is not unexpected. *In vivo* PET scans with the CD80 tracer [^{11}C]AM7 revealed an uptake in murine atherosclerotic plaques. No accumulation was found for [^{18}F]AC74. The detected difference between plaque and background uptake for [^{11}C]AM7 is substantially smaller than that for [^{18}F]FDG or [^{18}F]FDM, and in contrast to the metabolic tracers, significant levels were not reached at each time point. The more than sevenfold lower SUV value of [^{11}C]AM7 than that of the glucose analogs represents a critical drawback for atherosclerosis imaging since a high tracer uptake in plaques is required to detect the small lesions. The striking difference in absolute SUV may result in various factors. The most relevant may be the differences in uptake mechanisms. While [^{11}C]AM7 accumulates by reversible binding to its target, the metabolic tracers are trapped within the cells and accumulate quasi-irreversibly. An additional factor may be the lower abundance of classically activated M1 macrophages and additionally dendritic cells in plaques, both CD80-positive, compared to the overall number of metabolically active monocytes and macrophages that are targeted by [^{18}F]FDG and [^{18}F]FDM. Radiometabolite studies revealed only intact [^{11}C]AM7 at 30 min post injection [11]. The complete lack of [^{18}F]AC74 accumulation would be consistent with its 10-fold lower affinity to CD80. Based on the disappointing results with this tracer, we did not further investigate on its pharmacokinetic properties.

According to similar levels of CD80 mRNA over time and CD80 protein detected by FACS, we expected to have similar SUV values from 9 to 15 weeks post surgery. This was not the case, and we can only speculate on the low sensitivity and detection limit of PET. Even more, the specific activity of radiotracers is crucial in targeting receptors at low expression level. Both glucose analogs showed in this study comparable *in vivo* results and accumulated in atherosclerotic plaques US and DS of the cuff consistent with previous data demonstrating a similar accumulation of [^{18}F]FDG and [^{18}F]FDM in atherosclerotic regions of a rabbit model and a rat inflammatory model [17, 28]. These findings indicate that the impact of [^{18}F]FDM binding to MMR is insignificant, in agreement with the low *MRC1* gene expression in atherosclerotic segments of this mouse model.

Significant accumulation due to binding to the receptor would require a high affinity in the low nanomolar range and high specific activity, both not shown for [^{18}F]FDM. Therefore, presumably, both [^{18}F]FDG and [^{18}F]FDM accumulate predominantly in macrophages via intracellular trapping which would explain the similar *in vivo* results. Based on this *in vivo* data, the use of the mannose isomer [^{18}F]FDM does not present an advantage over [^{18}F]FDG for atherosclerosis imaging.

Conclusions

Atherosclerotic plaques of the ApoE KO-cuff mouse model displays significant CD80 levels which is comparable to human atherosclerosis and is of particular interest as it allows investigating inflammatory processes in advanced plaque in a preclinical model. It further enables the preclinical imaging of CD80-positive hot spots in atherosclerosis. The CD80-targeting tracers evaluated in this work had a considerably lower plaque uptake than the glucose-derived metabolic tracers. Optimizations regarding binding affinity and pharmacokinetic properties may improve their accumulation in atherosclerotic plaques.

Limitations of this Study

First, the animal model used in combination with the radiotracers included in this study implies that animal number is, in general, a critical factor since the reproducibility in this mouse model is low and the variability is high. In further studies, it is essential to use appropriate animal numbers to test specific hypotheses allowing sufficient statistical power. Second, murine atherosclerotic plaques are small with a size around the resolution limit of current preclinical PET systems. Therefore, it can be assumed that the partial volume effect influences the detected PET signal and the measured activity in plaques might be underestimated. Third, the extensive perivascular inflammation reactions in the cuff and control carotid segments could affect radiotracer accumulation. We minimized this artifact by monitoring the mice with [^{18}F]FDG after surgery (data not shown).

Acknowledgments. The authors thank Bruno Mancosu and Sabina Wunderlin for the technical support and helpful advice. We thank Dr. Michael Kuhlmann and Dirk Reinhardt from the European Institute for Molecular Imaging (EIMI, Münster, Germany) for introducing us to the shear stress-induced atherosclerosis mouse model and surgical training. We thank Dr. Cristina Müller (PSI, Villigen) for providing access to the Fuji ChemDri instrument and teaching sublingual blood collection. Ante Brekalo is acknowledged for the support in FDM synthesis. We appreciate the statistical advice by the statistical consultant of ETH. The authors acknowledge the support of the Scientific Center for Optical and Electron Microscopy (ScopeM) of the ETH Zurich. This work was financially supported by the Clinical Research Priority Program (CRPP) of the University of Zurich on Molecular Imaging (MINZ).

Author Contributions. R.M. conceived of and designed the experiments; established and performed all animal experiments, *ex vivo* staining, *ex vivo* PET, FACS, and qPCR; analyzed the data; and wrote the manuscript. L.S. performed the qPCR experiments and *ex vivo* staining and analyzed the data. N.B. supervised and analyzed the immunohistochemistry experiments. L.M. established the FDM chemistry and radiolabeling of ^{18}F-FDM and was involved in the discussion of results. C.K. established and conducted all animal surgeries and *in vivo* PET scans. A.C. performed the organic synthesis of the AC74 precursor and reference compounds and radiolabeling of [^{18}F]AC74. E.R. and C.H. conducted and analyzed the FACS experiments. S.M.A. and R.S. were involved in the discussion of results and revision of the manuscript. S.D.K. contributed to the supervision and planning of the experiments and revised the manuscript. A.M.H. supervised the study, experimental planning, and data interpretation and contributed to and supervised the manuscript writing.

Compliance with Ethical Standards

Conflict of Interest

The authors declare that they have no conflict of interest.

References

1. Pedersen EM, Oyre S, Agerbaek M, et al. (1999) Distribution of early atherosclerotic lesions in the human abdominal aorta correlates with wall shear stresses measured *in vivo*. Eur J Vasc Endovasc Surg 18:328–333
2. Chiu JJ, Chien S (2011) Effects of disturbed flow on vascular endothelium: pathophysiological basis and clinical perspectives. Physiol Rev 91:327–387
3. Chatzizisis YS, Coskun AU, Jonas M, et al. (2007) Role of endothelial shear stress in the natural history of coronary atherosclerosis and vascular remodeling: molecular, cellular, and vascular behavior. J Am Coll Cardiol 49:2379–2393
4. Andreou I, Antoniadis AP, Shishido K, et al. (2015) How do we prevent the vulnerable atherosclerotic plaque from rupturing? Insights from *in vivo* assessments of plaque, vascular remodeling, and local endothelial shear stress. J Cardiovasc Pharmacol Ther 20:261–275
5. Rogers IS, Nasir K, Figueroa AL, et al. (2010) Feasibility of FDG imaging of the coronary arteries: comparison between acute coronary syndrome and stable angina. JACC Cardiovasc Imaging 3:388–397
6. Tawakol A, Migrino RQ, Bashian GG, et al. (2006) *In vivo* 18F-fluorodeoxyglucose positron emission tomography imaging provides a noninvasive measure of carotid plaque inflammation in patients. J Am Coll Cardiol 48:1818–1824
7. Gaemperli O, Shalhoub J, Owen DR, et al. (2012) Imaging intraplaque inflammation in carotid atherosclerosis with 11C-PK11195 positron emission tomography/computed tomography. Eur Heart J 33:1902–1910
8. Rominger A, Saam T, Vogl E, et al. (2010) *In vivo* imaging of macrophage activity in the coronary arteries using 68Ga-DOTATATE PET/CT: correlation with coronary calcium burden and risk factors. J Nucl Med 51:193–197
9. Beer AJ, Pelisek J, Heider P, et al. (2014) PET/CT imaging of integrin alphavbeta3 expression in human carotid atherosclerosis. JACC Cardiovasc Imaging 7:178–187
10. Dweck MR, Chow MW, Joshi NV, et al. (2012) Coronary arterial 18F-sodium fluoride uptake: a novel marker of plaque biology. J Am Coll Cardiol 59:1539–1548
11. Müller A, Mu L, Meletta R, et al. (2014) Towards non-invasive imaging of vulnerable atherosclerotic plaques by targeting co-stimulatory molecules. Int J Cardiol 174:503–515
12. Cheng C, Tempel D, van Haperen R, et al. (2006) Atherosclerotic lesion size and vulnerability are determined by patterns of fluid shear stress. Circulation 113:2744–2753
13. Cheng C, Tempel D, van Haperen R, et al. (2007) Shear stress-induced changes in atherosclerotic plaque composition are modulated by chemokines. J Clin Invest 117:616–626
14. Kuhlmann MT, Cuhlmann S, Hoppe I, et al. (2012) Implantation of a carotid cuff for triggering shear-stress induced atherosclerosis in mice. J Vis Exp.

15. Wenning C, Kloth C, Kuhlmann MT, et al. (2014) Serial F-18-FDG PET/CT distinguishes inflamed from stable plaque phenotypes in shear-stress induced murine atherosclerosis. Atherosclerosis 234:276–282
16. Winkel LC, Groen HC, van Thiel BS, et al. (2013) Folate receptor-targeted single-photon emission computed tomography/computed tomography to detect activated macrophages in atherosclerosis: can it distinguish vulnerable from stable atherosclerotic plaques? Mol Imaging 12:1–5
17. Tahara N, Mukherjee J, de Haas HJ, et al. (2014) 2-deoxy-2-[18F]fluoro-D-mannose positron emission tomography imaging in atherosclerosis. Nat Med 20:215–219
18. Maganto-Garcia E, Tarrio M, Lichtman AH (2012) Mouse models of atherosclerosis. Chapter 15: Unit 15 24 11–23.
19. Kapourchali FR, Surendiran G, Chen L, et al. (2014) Animal models of atherosclerosis. World J Clin Cases 2:126–132
20. Hartwig H, Silvestre-Roig C, Hendrikse J, et al. (2015) Atherosclerotic plaque destabilization in mice: a comparative study. PLoS One 10:e0141019
21. Lardenoye JH, Delsing DJ, de Vries MR, et al. (2000) Accelerated atherosclerosis by placement of a perivascular cuff and a cholesterol-rich diet in ApoE*3Leiden transgenic mice. Circ Res 87:248–253
22. Smedby O (1997) Do plaques grow upstream or downstream?: an angiographic study in the femoral artery. Arterioscler Thromb Vasc Biol 17:912–918
23. Ylä-Herttuala S, Bentzon JF, Daemen M, et al. (2011) Stabilisation of atherosclerotic plaques. Position paper of the European Society of Cardiology (ESC) Working Group on atherosclerosis and vascular biology. Thromb Haemost 106:1–19
24. van Bochove GS, Paulis LE, Segers D, et al. (2011) Contrast enhancement by differently sized paramagnetic MRI contrast agents in mice with two phenotypes of atherosclerotic plaque. Contrast Media Mol Imaging 6:35–45
25. van der Heiden K, Hoogendoorn A, Daemen MJ, Gijsen FJ (2016) Animal models for plaque rupture: a biomechanical assessment. Thromb Haemost 115:501–508
26. Winkel LC, Hoogendoorn A, Xing R, et al. (2015) Animal models of surgically manipulated flow velocities to study shear stress-induced atherosclerosis. Atherosclerosis 241:100–110
27. Bessell EM, Thomas P (1973) The deoxyfluoro-D-glucopyranose 6-phosphates and their effect on yeast glucose phosphate isomerase. Biochem J 131:77–82
28. Furumoto S, Shinbo R, Iwata R, et al. (2013) *In vitro* and *in vivo* characterization of 2-deoxy-2-18F-fluoro-D-mannose as a tumor-imaging agent for PET. J Nucl Med 54:1354–1361
29. Wolfs IM, Donners MM, de Winther MP (2011) Differentiation factors and cytokines in the atherosclerotic plaque micro-environment as a trigger for macrophage polarisation. Thromb Haemost 106:763–771
30. Chinetti-Gbaguidi G, Baron M, Bouhlel MA, et al. (2011) Human atherosclerotic plaque alternative macrophages display low cholesterol handling but high phagocytosis because of distinct activities of the PPARgamma and LXRalpha pathways. Circ Res 108:985–995
31. Cho KY, Miyoshi H, Kuroda S, et al. (2013) The phenotype of infiltrating macrophages influences arteriosclerotic plaque vulnerability in the carotid artery. J Stroke Cerebrovasc Dis 22:910–918
32. Wilson HM (2010) Macrophages heterogeneity in atherosclerosis - implications for therapy. J Cell Mol Med 14:2055–2065